World Academy of Science, Engineering and Technology
International Journal of Chemical and Molecular Engineering
Vol:10, No:2, 2016

Structural and Electrochemical Characterization of Columnar-Structured Mn-Doped $Bi_{26}Mo_{10}O_{69-d}$ Electrolytes

Maria V. Morozova, Zoya A. Mikhaylovskaya, Elena S. Buyanova, Sofia A. Petrova, Ksenia V. Arishina, Robert G. Zaharov

***Abstract*—**The present work is devoted to the investigation of two series of doped bismuth molybdates: $Bi_{26-2x}Mn_{2x}Mo_{10}O_{69-d}$ and $Bi_{26}Mo_{10-2y}Mn_{2y}O_{69-d}$. Complex oxides were synthesized by conventional solid state technology and by co-precipitation method. The products were identified by powder diffraction. The powders and ceramic samples were examined by means of densitometry, laser diffraction, and electron microscopic methods. Porosity of the ceramic materials was estimated using the hydrostatic method. The electrical conductivity measurements were carried out using impedance spectroscopy method.

***Keywords*—**Bismuth molybdate, columnar structures, impedance spectroscopy, oxygen ionic conductors.

I. Introduction

THE Bi_2O_3-based complex oxides are rather interesting objects for fundamental and practical science research. They show ion-conductive, catalytic, ferroelectric, magnetic properties [1], [2] and different structural types, such as fluorite-related structures, pillar or layered Aurivillius phases or one-dimensional phases [1]-[4]. The last one includes columnar type compounds, such as $Bi_{26}Mo_{10}O_{69-d}$ -based solid solutions. The parent compound is a mono-dimensional oxide-ion conductor built of covalent $[Bi_{12}O_{14}]_n$ columns extending along the [010] direction and separated by a highly disordered metal-oxygen polyhedra and isolated Bi ions [4], [5].

$Bi_{26}Mo_{10}O_{69-d}$ ($Bi_{13}Mo_5O_{34.5-d}$) was first described by Buttery et al. [4] as a part of Bi-rich part of Bi-Mo-O system with Bi:Mo ratios ranging from 2.6 to 2.8. Vannier et al. [5] identified a $Bi_{26}Mo_{10}O_{69-d}$- type in the Bi_2O_3−MoO_3 system in a small solid solution range ($2.57 \leq Bi/Mo \leq 2.77$). More recently, [6] showed a number of room temperature stable bismuth molybdates with the Bi:Mo ratio 2.67 to 3.4 (i.e. 57.1% to 63.6% Bi_2O_3), which decay to the $Bi_{26}Mo_{10}O_{69-d}$ -type columnar structure at temperatures above ca. 920 K.

$Bi_{26}Mo_{10}O_{69-d}$ crystallizes above 580-585 K in monoclinic symmetry; triclinic symmetry is observed below 585 K. The structure of the monoclinic form was described in [5] with the following unit cell parameters: $a = 11.74$, $b = 5.80$, $c = 24.79$ Å, $\beta = 102.84°$ with $P2/c$ space-group symmetry. The monoclinic model includes columns, Bi ions and MoO_4 tetrahedra, giving the total quantity of oxygen positions equal to 68 per one unit cell. The structure of the triclinic form with additional oxygen position was suggested in [7]. It includes MoO_5 polyhedra and MoO_5-MoO_4 chains.

$Bi_{26}Mo_{10}O_{69-d}$ -based solid solutions can be obtained by substitution of Mo or Bi sites that leads to the formulae: $Bi_{26-2x}Me'_{2x}Mo_{10-2y}Me''_{2y}O_{69-d}$ (Me', Me'' – substituting ions). They show fast oxygen ionic conduction and photocatalytic properties. The substitution of $Bi_{26}Mo_{10}O_{69-d}$ may be carried out by doping of Bi-O sublattice or Mo-O sublattice or by double substitution. The $Bi_{26}Mo_{10-2y}Me''_{2y}O_{69-\delta}$ ($Bi_{13}Mo_{5-y}Me''_yO_{34\pm d}$) solid solutions were synthesized with 4 or 6 coordinated dopants [5] such as Me''= Li, Mg, Al, Si, Ge [8]; V, P, W [9]. The compounds with formulae $Bi_{26-2x}Me'_{2x}Mo_{10}O_{69-d}$ ($Bi_{13-x}Me'_xMo_5O_{34\pm d}$) were described for 8-coordinated dopants [5], such as Pb [10]; Ln [11]; Ca, Sr, Ba [9]. Double substituted $Bi_{26}Mo_{10}O_{69}$ was described for (Ca, $Sr)_2Bi_{24}Mo_8(Cr, W)_2O_{68}$ by [12]. In all described cases the substitution of isolated Bi ion occured. The substitution in $[Bi_{12}O_{14}]_n$ sublattice was revealed only for the Te dopant [13], [14]. It can be observed only for high Te concentration and causes formation of additional $[Bi_{12-x}Te_xO_{14}]_n$ columns.

Changes in electrical conductivity and catalytic properties, both positive and negative, result from these substitutions. The present work is devoted to synthesis, investigation and comparison of new Mn-substituted $Bi_{26}Mo_{10}O_{69-d}$. Manganese can show different oxidation state and coordination number and any of the two described types of substitution ($Bi_{26-2x}Mn_{2x}Mo_{10}O_{69-d}$ or $Bi_{26}Mo_{10-2y}Mn_{2y}O_{69-d}$).

II. Experimental

Polycrystalline samples of the compositions $Bi_{26-2x}Mn_{2x}Mo_{10}O_{69-d}$ and $Bi_{26}Mo_{10-2y}Mn_{2y}O_{69-d}$ ($0.0 \leq x, y \leq 1$) were synthesised by conventional solid state methods from the precursor oxides. Stoichiometric amounts of dried powders of Bi_2O_3 (99.9%), MoO_3 (99.5%), MnO (99.7%) were weighed and thoroughly grounded in an agate mortar with the ethanol as a homogenizer. The dried mixture was pelletized at 20 bar using a uniaxial press yielding pellets of 20 mm in diameter. The pellets were placed on an alumina plate on the "powder

M. V. Morozova is with Ural Federal University, Lenin Ave.51, 620000, Yekaterinburg, Russia (phone: 83432617553; e-mail: maria.morozova@urfu.ru).

Z. A. Mikhaylovskaya, E. S. Buyanova and K.V. Arishina are with Ural Federal University, Lenin Ave.51, 620000, Yekaterinburg, Russia (e-mail: zozoikina@mail.ru, elena.buyanova@urfu.ru, arishina.ksenya@mail.ru).

S. A. Petrova and R. G. Zaharov are with Institute for Metallurgy UD RAS, Amundsen street, 101, 620016, Yekaterinburg, Russia (e-mail: danaus@mail.ru, danaus@yandex.ru).

bed" and heated at 823 K for 48 h, then quenched in water to room temperature. The samples were then regrinded in ethanol, dried, pelletized again and reheated to 1123 K for 24 h, followed by slow cooling in air to room temperature over a period of approximately 12 h.

The dopant concentration ranges of $Bi_{26-2x}Mn_{2x}Mo_{10}O_{69-d}$ and $Bi_{26}Mo_{10-2y}Mn_{2y}O_{69-d}$ solid solutions and crystal forms were determined by XRPD. X-ray powder diffraction data were obtained on a Bruker Advance D8 diffractometer with a VANTEC1 detector, Ni filtered Cu Kα radiation (λ_1 = 1.54056 Å and λ_2 = 1.54439 Å). Data were collected in flat plate θ/θ geometry and calibrated against external Si standards.

The grain size of the powders was estimated by a nanoparticle size analyzer (Shimadzu SALD-7101). The morphology of the obtained powders and their chemical composition were studied using a JEOL JSM 6390LA with EDX-analyzer JED 2300. Chemical analysis of the samples was realized by atomic emission and atomic absorption spectroscopy analysis of dissolved powders of bismuth molybdates on an iCAP 6500 Duo and Solaar M6 (Thermo Scientific) by both standard addition and calibration curve methods.

Hydrostatic weighting was used for investigation of the density of ceramic pellets coated with a moisture-resistant coating. The volume (geometric) porosity of ceramic samples was obtained by comparison of experimental and theoretical (X-ray) density values of the samples.

For the impedance measurements the synthesised samples were pelletized at 20 bar yielding pellets of 10 mm in diameter and ca. 2.5 mm thick. The pressed pellets were then heated to 1123 K for 24 h, and then slowly cooled in air to room temperature. Pt electrodes were applied by decomposition of $NH_4(PtCl_6)$ dispersion at *ca*. 673 K. The impedance measurements were carryed out in the range of 523-1123 K on Elins Z-3000 impedance spectrometer over the frequency range of 3 MHz to 10 Hz. For the analysis of the impedance plots the equivalent electrical circuits method was used (Zview software, Version 2.6b, Scribner Associates, Inc.).

III. Results and Discussion

A. Crystal Structure

The XPRD measurements showed formation of the single-phase $Bi_{26-2x}Mn_{2x}Mo_{10}O_{69-d}$ and $Bi_{26}Mo_{10-2y}Mn_{2y}O_{69-d}$ complex oxides up to x=0.8 and y=0.2. SEM measurement confirmed these homogeneity ranges. The high dopant content ($x \geq 0.40$ and y=0.2) leads to stabilization of the monoclinic form of $Bi_{26-2x}Mn_{2x}Mo_{10}O_{69-d}$. The unit cell parameters of $Bi_{26-2x}Mn_{2x}Mo_{10}O_{69-d}$ show a good correlation with the Vegard's law (Table I, Fig. 1).

TABLE I
Cell Parameters of Mn-Doped $Bi_{26}Mo_{10}O_{69-D}$ (Present Work) and Some $Bi_{26}Mo_{10}O_{69-D}$-Based Solid Solutions [5]

Composition	a±0.002, Å	b±0.001, Å	c±0.005, Å	α±0.02, °	β±0.02, °	γ±0.02, °	V (Å^3)
$Bi_{25.8}Mn_{0.2}Mo_{10}O_{69-d}$	11.774	5.801	24.744	89.8	102.63	89.88	1649.10
$Bi_{25.6}Mn_{0.4}Mo_{10}O_{69-d}$	11.734	5.800	24.734	89.88	102.19	89.92	1645.40
$Bi_{25.4}Mn_{0.6}Mo_{10}O_{69-d}$	11.728	5.793	24.693	90.00	102.17	89.85	1639.90
$Bi_{25.2}Mn_{0.8}Mo_{10}O_{69-d}$	11.703	5.787	24.680	90.00	102.17	90.00	1633.90
$Bi_{25.0}Mn_{1.0}Mo_{10}O_{69-d}$	11.693	5.780	24.672	90.00	102.17	90.00	1630.00
$Bi_{24.8}Mn_{1.2}Mo_{10}O_{69-d}$	11.681	5.775	24.652	90.00	102.18	90.00	1625.50
$Bi_{24.6}Mn_{1.4}Mo_{10}O_{69-d}$	11.669	5.769	24.638	90.00	102.24	90.00	1620.89
$Bi_{24.4}Mn_{1.6}Mo_{10}O_{69-d}$	11.654	5.763	24.615	90.00	102.27	90.00	1615.43
$Bi_{26}Mo_{9.8}Mn_{0.2}O_{69-d}$	11.749	5.800	24.789	89.89	102.68	89.92	1648.00
$Bi_{26}Mo_{9.6}Mn_{0.4}O_{69-d}$	11.735	5.801	24.793	90.00	102.77	90.00	1645.75
$Bi_{27}Mo_{10}O_{69-d}$ [5]	11.771	5.801	24.772	89.96	102.91	89.93	1648.76
$Bi_{27.5}Mo_{10}O_{69-d}$ [5]	11.741	5.801	24.782	90.00	102.81	90.00	1645.90

As a result, we observe the formation of single phase powder samples by using either of the two substitution ways. It can be explained from two points of view:

(1) Mixed oxidation state of Mn in complex oxide provides different types of coordination (4 and 8);
(2) Only doping of Bi-O sublattice occurs, the existence of the $Bi_{26}Mo_{10-2y}Mn_{2y}O_{69-d}$ ($y \leq 0.2$) is a result of forming the $Bi_{26}(Mo_{10-z}Bi_z)O_{69-d}$-based solid solutions [5].

We believe that here only substitution of Bi atoms occurs. This hypothesis is corroborated by the ranges of $Bi_{26}Mo_{10}O_{69-d}$ solid solution e.g. y=0.2 composition results in $Bi_{26}Mo_{10.6}Mn_{0.4}O_{69-d}$ composition that corresponds to the ratio (Bi+Mn)/Mo=2.75; y=0.1 composition leads to $Bi_{26}Mo_{10.8}Mn_{0.2}O_{69-d}$ composition that corresponds to ratio (Bi+Mn)/Mo=2.67. Both mentioned ratios are in the solid solution range described by [5] ($2.57 \leq Bi/Mo \leq 2.77$). The compositions mentioned (y=0.1 and y=0.2) also show unit cell parameters similar to that of the Bi/Mo>2.6 solid solutions (Table I, [5]). The same phenomenon was observed for Mg-doping, when solid solutions ranges was determined up to x=0.4 [15] and y=0.25 [8] and Co (to x, $y \leq 0.2$ [16]). It should be noted that in spite of the difference of ionic radii of Bi, Mo and any dopant element the compression of the unit cell is observed The Rietveld analysis is not effective for the occupancy calculation due to proximity of Bi and Mn mass attenuation coefficient for CuKα radiation. Thus we can say that x-doping leads to substitution of Bi, but the way of substitution of y-doping is not obvious, therefore in the present

paper we consider mostly the *x*-doped compositions.

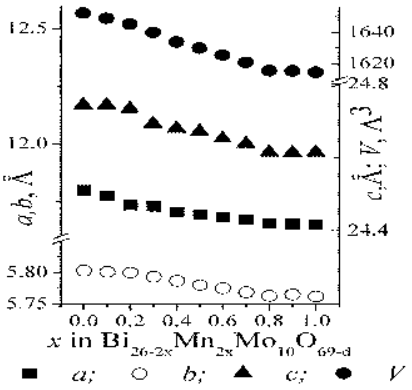

Fig. 1 The Unit cell parameters visualization for the $Bi_{26-2x}Mn_{2x}Mo_{10}O_{69-d}$ compositions

B.Morphological Characteristics of the Powder and Ceramic Samples

The particle sizes of the synthesized powders were determined to be in the range of 1-10 μm Fig. 2 (a). After the final annealing of the powders the pellets were formed and annealed at 1123 K for 12 hours. As an example the SEM images of the surface and cross-section of $Bi_{26-2x}Mn_{2x}Mo_{10}O_{69-d}$ ceramic samples are shown in Figs. 2 (b) and (c). Scanning electron microscopy showed essential grain growth. Large grains (about dozens of microns) and isolated spherical pores are seen in Figs. 2 (b) and (c), indicating the formation of dense, massive ceramics.

TABLE II
EXAMPLES OF CHEMICAL ANALYSIS OF MN-SUBSTITUTED $Bi_{26}Mo_{20}O_{69-D}$

Compound	Theoretical Ratio of Bi:Mn:Mo	Experimental Ratio of Bi:Mn:Mo, (x±0.40:y±0.10:z±0.05)
$Bi_{13}Mo_5O_{34\pm\delta}$	13.00: 0.00: 5.00	12.97: 0.00:5.00
$Bi_{25.8}Mn_{0.2}Mo_{10}O_{69-d}$	12.90: 0.10: 5.00	13.15: 0.11: 4.94
$Bi_{25.6}Mn_{0.4}Mo_{10}O_{69-d}$	12.80: 0.30: 5.00	13.11: 0.23: 4.94
$Bi_{25.4}Mn_{0.6}Mo_{10}O_{69-d}$	12.70: 0.30: 5.00	12.85: 0.36: 4.94
$Bi_{25.2}Mn_{0.8}Mo_{10}O_{69-d}$	12.60: 0.40: 5.00	12.98: 0.37: 4.94
$Bi_{25.0}Mn_{1.0}Mo_{10}O_{69-d}$	12.50: 0.50: 5.00	12.87: 0.51: 4.94

TABLE III
EXAMPLES OF DENSITY MEASUREMENTS OF MN-SUBSTITUTED $Bi_{26}Mo_{20}O_{69-D}$

Compound	Density of ceramic samples		
	Theoretical density	Experimental density (±0.02)	Porosity, %
$Bi_{13}Mo_5O_{34\pm\delta}$	7.52	7.34	2
$Bi_{25.8}Mn_{0.2}Mo_{10}O_{69-d}$	7.52	7.45	1
$Bi_{25.6}Mn_{0.4}Mo_{10}O_{69-d}$	7.50	7.46	1
$Bi_{25.4}Mn_{0.6}Mo_{10}O_{69-d}$	7.49	7.44	1
$Bi_{25.2}Mn_{0.8}Mo_{10}O_{69-d}$	7.49	7.25	3
$Bi_{25.0}Mn_{1.0}Mo_{10}O_{69-d}$	7.47	7.46	1
$Bi_{24.8}Mn_{1.2}Mo_{10}O_{69-d}$	7.46	7.30	2
$Bi_{24.6}Mn_{1.4}Mo_{10}O_{69-d}$	7.45	7.38	1
$Bi_{24.4}Mn_{1.6}Mo_{10}O_{69-d}$	7.44	7.28	2

The concentrations of the manganese obtained from EDX measurements were found to be similar to the corresponding theoretical values. The variations in manganese content from one grain to another may be attributed to normally higher error of EDX analysis for low concentration of the elements. The concentration of Bi and Mo couldn't be determined correctly because of overlapping of their spectral lines.

The results of chemical analysis realized by AAS and AES-ICP methods are shown in Table II. The concentrations of all dopants confirm the theoretical formulae within the experimental errors. The method of calibration curves was determined to be not suitable for Mn determination because of large Bi concentration in the solution. The standard addition methods compensated Bi and can be recommended for chemical analysis of such materials.

Hydrostatic weighting study showed high density of the sintered pellets, experimental density reaches values more than 97% of theoretical (X-ray) density (Table III).

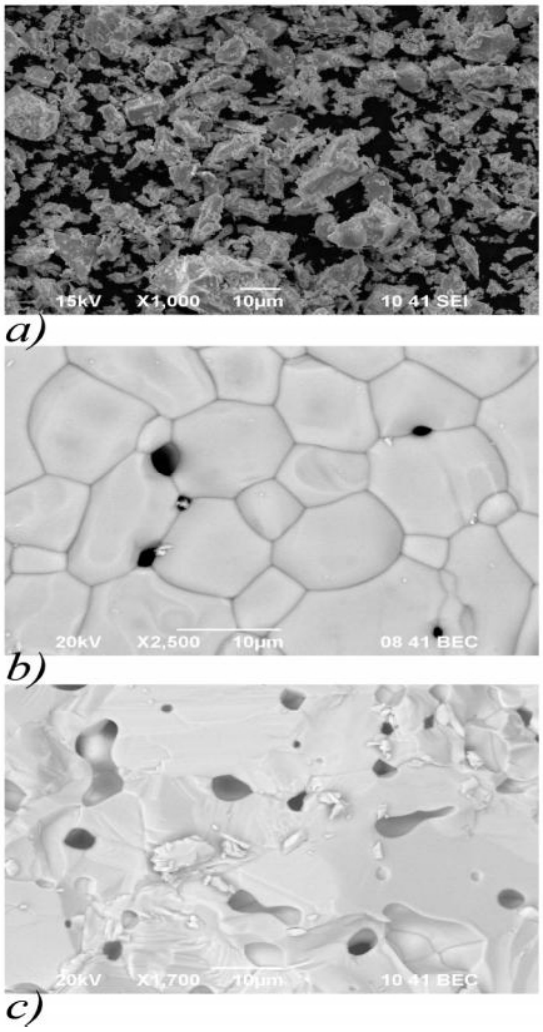

Fig. 2 SEM images for $Bi_{26-2x}Mn_{2x}Mo_{10}O_{69-d}$: (a) - x=0.2, powder, secondary electrons imaging, scale 1:1000; (b) x=0.6, ceramic pellet surface, backscattering electrons imaging, scale 1:2500; (c) x=0.6, ceramic pellet cross-section, backscattering electrons imaging, scale 1:1700

C.Electrical Conductivity

The impedance spectroscopy was used for investigation of electro-conductive properties of the ceramic samples of Mn-substituted $Bi_{26}Mo_{10}O_{69-d}$. For the analysis of impedance plots the equivalent electrical circuits method was used (Zview software, Version 2.6b, Scribner Associates, Inc.). Figs. 3 (a) and (b) show examples of complex plane plots of $Bi_{25.8}Mn_{0.6}Mo_{10}O_{69-d}$ at different temperatures. In general, this shape of complex plane plots is typical for all studied compositions. Equivalent electrical circuits were obtained by using a complex nonlinear least square. For every temperature it gave the good agreement of calculated and experimental impedance curves (Figs. 3 (a) and (b)). It can be seen that the shape of the complex plane plots appears to be different in different temperature regions. In general, two types of complex plane plots can be described, at relatively high temperatures and at relatively low temperatures. High temperature spectra were characterized by depressed unsymmetrical semi-circle (Fig. 3 (a)). The total resistivity of the sample corresponds to the high frequency intercept of it. The depressed semi-circle can be described by two linked parallel R-CPE connections (R is resistor; CPE is constant phase element). The CPE capacity parameters are about 10^{-5}-10^{-6} F, therefore R-CPE parallel connections correspond to electrochemical processes at the electrodes [17] (they are named as R el1, CPE el1 and R el2, CPE el2 at equivalent electrical circuits at Fig. 3 (a)).

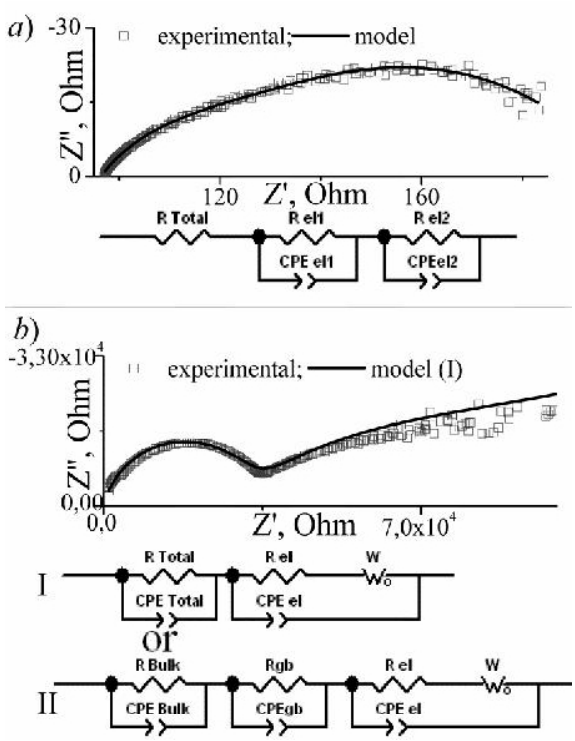

Fig. 3 Impedance plots and equivalent electrical circuits of x=0.3 compound: (a) high temperature region; (b) low temperature region

Low temperature spectra are characterized by a slightly depressed symmetrical (model I) or unsymmetrical (model II) semi-circle in the high and medium frequency part, which represents the total resistivity of the sample, associated to straight lines at low frequencies. These straight lines generally describe the complicated ionic transport and processes at the electrodes interface (Fig. 3 (b)). The symmetry of high-frequency semi-circle shows the strong dependence from dopant concentration (Fig. 4). For compounds with low Mn-content only one semi-circle is observed, but for the samples with larger Mn concentration the semi-circle becomes unsymmetrical and can be described by two semi-circles (Fig. 4). Therefore, two equivalent models were suggested (*I* and *II* in Fig. 3 (b)). Model *I* describes the total resistivity of $Bi_{26-2x}Mn_{2x}Mo_{10}O_{69-d}$ with low Mn content ($x \leq 0.5$), while model *II* describes combination of the bulk and grain boundary resistivity of Mn-rich complex oxides ($0.5 < x \leq 0.8$) (Fig. 3 (b)). The corresponding CPE capacity values in R-CPE connections are about 10^{-11} F for "CPE bulk" and 10^{-10} F for "CPE grain boundary", which are typical capacity values for polycrystalline samples [17]. Possible explanations of this phenomenon are 1) the presence of the second phase thin layer is not detected at room temperature (e.g. triclinic $Bi_{26}Mo_{10}O_{69-d}$ can cover grains of monoclinic $Bi_{26}Mo_{10}O_{69-d}$); 2) the preferred orientation of the grains (it can be indirectly confirmed by specific profile function at X-Ray diffractograms).

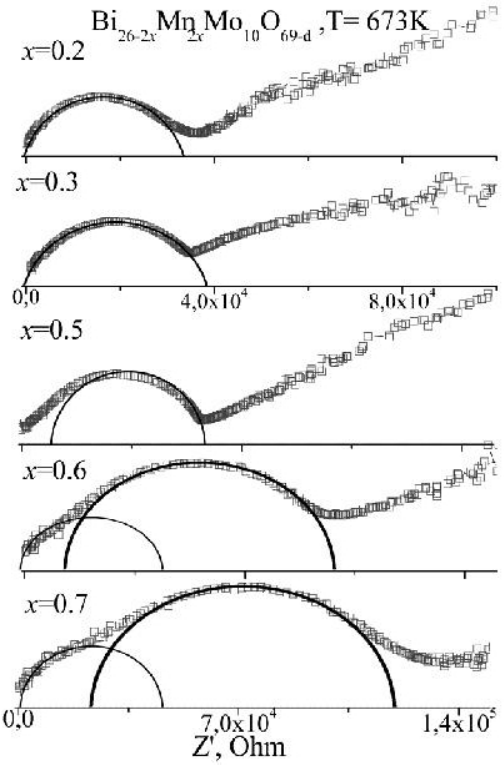

Fig. 4 High and medium frequency parts of the complex plane plots of $Bi_{26-2x}Mn_{2x}Mo_{10}O_{69-d}$. Evolution of the spectra shape vs. Mn concentration is shown

According to the results of the impedance measurements the temperature and concentration curves of electrical

conductivity of $Bi_{26-2x}Mn_{2x}Mo_{10}O_{69-d}$ ceramic samples were plotted. The characteristic Arrhenius plots (log (σ)-1000/T) have linear shape and activation energy values (0.5-0.95 eV) which is typical for oxygen-ion conductors. Figs. 5 (a) and (b) show characteristic temperature, dopant concentration and conductivity relationship of the Mn-substituted $Bi_{26}Mo_{10}O_{69-d}$. Two significant drops of the electrical conductivity associated with monoclinic-triclinic phase transition are observed only for the parent compound Fig. 5 (a). The temperature of the phase transition of triclinic $Bi_{26-2x}Mn_{2x}Mo_{10}O_{69-d}$ is below the range of measurement temperature thus only conductive properties of monoclinic form are observed. The activation energy of Mn-substituted $Bi_{26}Mo_{10}O_{69-d}$ increases with x from 0.5 to 0.80 eV. The concentration plots of the total electrical conductivity of $Bi_{26-2x}Mn_{2x}Mo_{10}O_{69-d}$ represent a parabolic dependence (Fig. 5 (b)). The highest conductivity in the series at all temperatures is detected for the $Bi_{25.4}Mn_{0.6}Mo_{10}O_{69-d}$ compound: $\sigma_{973K} = 2.8*10^{-3}$ S×cm^{-1} at 973 K and $\sigma_{623K} = 1.3*10^{-5}$ S×cm^{-1} at 673 K.

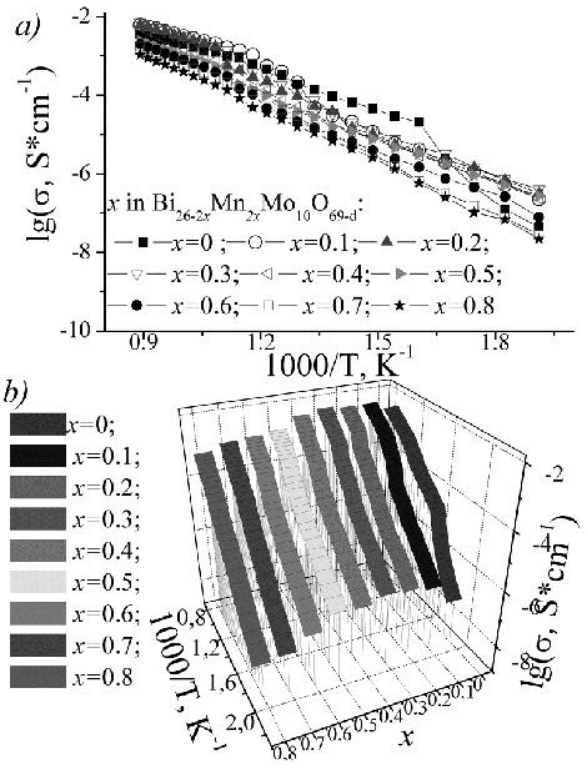

Fig. 5 (a) Characteristic Arrhenius plots of $Bi_{26-2x}Mn_{2x}Mo_{10}O_{69-d}$; (b) 3D characteristic temperature and concentration plots of total electrical conductivity of $Bi_{26-2x}Mn_{2x}Mo_{10}O_{69-d}$

IV. Conclusion

As a result of the present work the formation of single-phase $Bi_{26-2x}Mn_{2x}Mo_{10}O_{69-d}$ and $Bi_{26}Mo_{10-2y}Mn_{2y}O_{69-d}$ complex oxides up to x=0.8 and y=0.2 was shown. Dense and massive ceramics samples with low porosity (≤3%) were obtained. The electrical conductivity measurements were carried out using impedance spectroscopy and showed high ionic conductivity at $Bi_{26-2x}Mn_{2x}Mo_{10}O_{69-d}$. The maximum of conductivity in all temperatures is detected for $Bi_{25.4}Mn_{0.6}Mo_{10}O_{69-d}$.

Acknowledgment

This work was financially supported by the Russian Fund of Basic Research (project No 14-03-92605, project No 16-33-60026.); by the Ministry of Education and Science of Russian Federation (project N 4.1039.2014/K)

The equipment of the Ural Center for Shared Use "Modern nanotechnology" UrFU was used. The research was made possible in part by the Ministry of Education and Science of the Russian Federation (ID RFMEFI59414X0011).

References

[1] J. C. Boivin, "Structural and electrochemical features of fast oxide ion conductors," *Int. J. Inorg. Mat*., vol. 3, pp. 1261-1266, Dec. 2001.

[2] F. Abraham, J. C. Boivin, G. Mairesse and G. Nowogrocki, "The bimevox series: a new family of high performances oxide ion conductors*," Solid State Ionics*, vol. 40-41, pp. 934-937, Aug. 1990.

[3] R. Enjalbert, G. Hasselmann and J. Galy, "$(Bi_{12}O_{14}E_{12})n$ Columns and lone pairs E in $Bi_{13}Mo_4VO_{34}E_{13}$: synthesis, crystal structure, and chemistry of the Bi_2O_3–MoO_3–V_2O_5 system", *J. Solid State Chem.*, vol. 131, pp. 236-245, July 1997.

[4] D. J. Buttrey, T. Vogt, G. P. A Yap and A. L. Rheingold, "The structure of $Bi_{26}Mo_{10}O_{69}$", *Mater. Res. Bull*., vol. 32, no. 7, pp. 947-962, July 1997.

[5] R. N. Vannier, G. Mairesse, F. Abraham and G. Nowogrocki, "$Bi_{26}Mo_{10}O_\delta$ solid solution type in the Bi_2O_3–MoO_3–V_2O_5 ternary diagram", *J. Solid State Chem*. vol. 122, no.2, pp. 394-406, Mar. 1996.

[6] J. Galy, R. Enjalbert, P. Rozier and P. Millet, "Lone pair stereoactivity versus anionic conductivity. Columnar structures in the Bi_2O_3–MoO_3 system", *Solid State Sci*. vol. 5, no.1, pp. 165–174. Jan. 2003.

[7] C. D. Ling, W. Miiller, M. R. Johnson, D. Richard, S.Rols, J. Madge et al., "Local structure, dynamics, and the mechanisms of oxide ionic conduction in $Bi_{26}Mo_{10}O_{69}$", *Chem. Mater*. vol. 24, pp. 4607−4614, Nov. 2012.

[8] B. Bastide, S. Villain, P. Salles and J. Galy, "Oxygen diffusion pathway in the anionic conductor $Bi_{26}Mo_9GeO_{68}$", *Solid State Sci*. –vol. 4, no. 5, pp. 599-608, Apr. 2002.

[9] R. N. Vannier, S. Danzé., G. Nowogrocki, M. Huve and G. Mairesse, "A new class of mono-dimensional bismuth-based oxide anion conductors with a structure based on $(Bi_{12}O_{14})_\infty$ columns", *Solid State Ionics*, vol. 136-137, pp. 51-59. Nov. 2000.

[10] J. Galy, P. Salles, P. Rozier, A. Castro, "Anionic conductors $Ln_{2/3}(Bi_{12}O_{14})(MoO_4)_5$ with Ln=La, Nd, Gd, Ho, Yb. Synthesis–spark plasma sintering–structure–electric properties", *Solid State Ionics,* vol. 177, no. 33-34, pp. 2897-2902, Nov. 2006.

[11] R. Enjalbert, G. Hasselmann, J. Galy, "A new mixed oxide with $(Bi_{12}O_{14})_n$ columns: $PbBi_{12}Mo_5O_{34}$", *Acta Crystallgr. Sect.C*, vol. 53, no. 3, pp.. 269-272, Mar. 1997.

[12] B. Muktha, T. N. Guru Row, "Crystal structure and ionic conductivity of the series $A_2Bi_{24}Mo_8X_2O_{68}$ (A=Ca, Sr and Ba and X=Cr, W)", *Struct. Chem*., vol. 18, pp. 195-202, Dec. 2007.

[13] A. Castro, R. Enjalbert, P. Baules, J. Galy, "A. Synthesis and Structural Evolution of the Solid Solution $Bi(Bi_{12-x}Te_xO_{14})Mo_{4-x}V_{1+x}O_{20}$ ($0\leq x<2.5$)", *J. Solid State Chem*., vol. 139, no. 2, pp. 185-193, Aug. 1998.

[14] V. Thakral, N. Bhardwaj, S. Uma, "Synthesis and Structural Investigation of a Unique Columnar Phase in the Bi_2O_3−TeO_2−V_2O_5 System", *Inorg. Chem. (ACS)*, vol. 51, no. 3, pp. 1462−1470, Feb. 2012.

[15] Z. A. Mikhaylovskaya, E. S. Buyanova, M. V. Morozova, S. A. Petrova, R. G. Zakharov, I. V. Nikolaenko, I. Abrahams, "$Bi_{13-x}Me_xMo_5O_{34\pm\delta}$ (Me = Mg, Ca, Sr, Ba) solid solutions: synthesis and properties", *Ionics*, vol. 21, no. 8, pp. 2259-2268, Aug. 2015.

[16] . Z. A. Mikhailovskaya, E. S. Buyanova, S. A. Petrova, M. V. Morozova, V. M. Zhukovskiy, R. G. Zakharov, et al, "Cobalt-doped $Bi_{26}Mo_{10}O_{69}$: crystal structure and conductivity", *J. of Solid State Chem.*, vol. 204, pp. 9-15, August 2013.

[17] J. T. S. Irvine, D. C. Sinclair, A. R. West, "Electroceramics: Characterization by Impedance Spectroscopy", *Advanced Materials*. vol. 2, no. 3, pp. 132−138, Mar. 1990.